Profiling embryonic stem cell differentiation by MALDI-MS: development of a reproducible and robust sample preparation workflow

Rachel E. Heap[1], Anna Segarra-Fas[2], Greg M. Findlay[2] and Matthias Trost[1*]

[1]Institute for Cell and Molecular Biosciences, Newcastle University, Newcastle-upon-Tyne, UK; [2]MRC Protein Phosphorylation & Ubiquitylation Unit, University of Dundee, Dundee, Scotland, UK

ABSTRACT: MALDI-TOF mass spectrometry (MS) is widely used to characterize and biotype bacterial samples, but a complimentary method for profiling of mammalian cells is still underdeveloped. Current approaches vary dramatically in their sample preparation methods and are not suitable for high-throughput studies. In this work, we present a universal workflow for mammalian cell MALDI-TOF MS analysis and apply it to distinguish ground-state naïve and differentiating mouse embryonic stem cells (mESCs), which can be used as a model for drug discovery. We employed a systematic approach testing many parameters to evaluate how efficiently and reproducibly each method extracted unique mass features from four different human cell lines. This data enabled us to develop a unique mammalian cell MALDI-TOF workflow involving a freeze-thaw cycle, methanol fixing and CHCA matrix to generate spectra that yield maximum information and are highly reproducible. We applied our optimized workflow to distinguish naïve and differentiating populations using multivariate analysis and reproducibly identifying unique features. Consequently, our MALDI-TOF MS profiling method enables identification of unique biomarkers and robust phenotyping of mESC differentiation. This method can in the future be applied to profile other cell types and expanded towards cellular MALDI-TOF MS screening assays.

Matrix-assisted laser desorption/ionization time of flight mass spectrometry (MALDI-TOF-MS) is an versatile technique with many different applications ranging from protein identification by peptide mass fingerprinting and small molecule analysis to imaging of tissues.[1–3] Although conventionally considered a low-throughput technology, recent advances in MS and liquid handling technologies and liquid handling tools has enabled MALDI-TOF-MS to emerge as a promising tool for label-free high-throughput screening (HTS) within both the pharmaceutical industry and academic sphere.[4–6] This platform is already well established for *in vitro* assays to monitor post-translational modifications such as ubiquitylation,[7,8] phosphorylation[9,10] and methylation,[11,12] as the read-out is relatively simple with often just a single substrate and product. Similar to MALDI, laser desorption ionization can also be combined with self-assembled monolayers (SAMs), also known as SAMDI, and is proving to be a powerful technology in HTS drug discovery.[13,14] Substrates are first immobilized on a surface before treatment with an enzyme, thus determining activity and kinetic parameters. Interestingly, SAMDI has been shown to be not only compatible with peptide substrates for protein specificity,[15,16] but also carbohydrates and glycosyltransferase activity.[17]

Whole cell analysis or cellular assays for evaluating compound efficacy affecting a cellular phenotype presents an interesting challenge for MALDI-TOF MS analysis as the system becomes inherently more complex. A well-established application for whole cell MALDI-TOF MS is the profiling of micro-organisms, also known as biotyping.[18,19] Profiling of protein biomarkers specific to a bacterial taxonomy by MALDI-TOF MS was first performed by Claydon *et al* and enabled reproducible and robust identification of gram-positive and gram-negative species.[20] Since then, bacterial genera have been identified through various approaches from spectral mass fingerprinting, to more complex approaches that involve comparing peaks identified in MALDI spectra to predictive masses from proteomic and genomic data sets.[21,22] This in turn enabled the generation of reference protein databases that list biomarkers specific to different bacterial species.[23] Combined with automated spectral acquisition and novel algorithms to tackle data analysis, biotyping has become a powerful, high-throughput tool for rapidly profiling bacterial genera in both academic and clinical settings.[24] However, inter-lab studies revealed surprising discrepancies in *E. coli* fingerprints as experimental variables such as sample preparation and instrument parameters can affect spectral quality and reproducibility.[25,26] Several studies have therefore scrutinized sample preparation methods for bacterial biotyping, looking at solvent extraction or direct analysis, sample handling and also matrix choice affects spectra quality with the aim of developing a standardized method to enable universal identification of micro-organisms.[27–29]

While bacterial biotying has been very successful and has become a standard tool in the clinic, profiling of mammalian cells by MALDI-TOF MS has not yet reached this level. It has been used for phenotypic screening of human cancer cell lines,[30] identification of cells within a co-culture[31] or tissues[32] and detection of transient changes within a specific cell type, such as immune cells.[33–36] However, many of these studies list dramatically different experimental procedures with several being adapted from existing biotyping protocols. The huge range of experimental parameters could therefore be problematic for translation of published assays to the pharmaceutical industry.

To address the variation in experimental workflows we have systematically tested different methods at key steps in preparing

mammalian cells for whole cell MALDI-TOF MS analysis. We have generated a robust and sensitive sample preparation workflow by studying four commonly used human cell lines, followed by application of our final method to a pharmacologically controlled biological system, where we applied our optimized method to profile differences between naïve ground-state mouse embryonic stem cells (mESCs) and those undergoing differentiation. Thus, we have established a sample preparation method that is highly reproducible, robust and sensitive with respect to both biological and experimental variances and would be suitable for expansion to a HTS platform.

Materials and Methods

Chemicals. All reagents used for this study were of HPLC grade unless stated otherwise. Acetonitrile (ACN), water (H_2O), acetone, hexane, methanol (MeOH), dichloromethane (DCM), isopropanol were purchased from Merck (Darmstadt, GER). Cell lines U2OS, MCF7, THP1 and HEK293 were purchased from ATCC (Manassas, USA). Dulbecco's Modified Eagle Medium (DMEM), Roswell Park Memorial Institute medium (RPMI), phosphate buffered saline solution (PBS), fetal bovine serum (FBS), β-mercaptoethanol (cell culture grade) were all purchased from Gibco, Life Technologies (Darmstadt, Germany). L-glutamine and penicillin-streptomycin were purchased from Lonza (Basel, Switzerland). Trypsin-EDTA solution, trifluoroacetic acid (TFA) were purchased from Sigma Aldrich. Sinapinic Acid (SA), 2,5-dihydroxybenzoic Acid (DHB) and α-cyano-4-hydroxycinnamic acid (CHCA) were kindly provided by Bruker Daltonics (Bremen, Germany).

Human cell line culture. THP1 cells were cultured in suspension in RPMI-1640 medium supplemented with 10% FBS, 1% pen/strep, 1% L-glutamine and 50 µM β-mercaptoethanol and maintained at a concentration between 2.5×10^5 - 1×10^6 cells per milliliter to a maximum passage of 20. HEK293 and U2OS cell lines were cultured in DMEM media supplemented with 10% FBS, 1% pen/strep and 1% L-glutamine. MCF7 cells were cultured in RPMI-1640 media supplemented with 10% FBS, 1% pen/strep and 1% L-glutamine. Adherent cell lines (U2OS, MCF7 and HEK293) were lifted from 10 cm culture plates by addition of trypsin-EDTA solution before passaging 1:6 every two days to a maximum passage of 20. All cell lines were incubated in a controlled atmosphere at 5% CO_2 and 37°CCells were harvested and centrifuged at 300 xg for 3 minutes before resuspension in PBS and counted using a hemocytometer. Cells were then aliquoted at a concentration 1×10^6 into 1.5 mL microtubes and centrifuged at 300 xg, 4 °C for 10 minutes.

Mouse Embryonic Stem Cell (mESC) Culture. CGR8 mESCs were cultured in 0.1% gelatin [w/v] coated plates in N2B27 medium (DMEM/F12-Neurobasal (1:1), 0.5% N2, 1% B27 (ThermoFisher Scientific), 1% L-glutamine, 100 µM β-mercaptoethanol) containing "2i",[37] 3 µM CHIR99021 (Axon Medchem) and 1 µM PD0325901, in a controlled atmosphere at 5% CO_2 and 37°C. To induce multi-lineage differentiation,[38] cells were plated at 4×10^4 cells/cm^2 in N2B27 medium without CHIR99021 and PD0325901 and incubated for 48h at 5% CO_2 and 37°C.

RNA extraction and qPCR. Total RNA extraction was performed by a column-based system (Omega) and then subjected to reverse transcription using iScript reverse transcriptase (Bio-Rad) according to the manufacturer's guidelines. qPCR reactions were carried out using SYBR® Premix Ex Taq™ II Supermix (Takara) in a CFX384 real-time PCR system (Bio-Rad). Samples were analyzed for gene expression in 2i release conditions relative to 2i medium culture using the ΔΔCt method, and GAPDH expression was analyzed as a loading control. Data from three independent biological replicates, with two technical replicates f each, were analyzed in Excel software (Microsoft) and plotted in GraphPad Prism v.6.00 software (GraphPad). Primers used are listed in S-Table 1. Statistical significance was determined using an unpaired Student's t test, and significant differences were considered when $p < 0.05$.

Cell microscopy and diameter analysis. The four cell lines were measured for number and cell diameter by light microscopy using an Evos XL Core Cell Imaging System (Invitrogen). Optimal cell numbers were calculated by a cell titration, whose values are reported in Table 1, and these concentrations were used for subsequent experiments. To assess permeability, cell pellets were resuspended in PBS before mixing 1:1 with trypan blue. Trypan blue positive cells were then automatically counted using the same microscope to calculate cell viability. For mESC phenotype visualization, brightfield light microscopy was used in a Leica DM IL LED microscope at 10X magnification.

MALDI-TOF target preparation. AnchorChip (1536) and Ground steel (384) MALDI targets (Bruker, Bremen, Germany) were first cleaned thoroughly by submersion and sonication in isopropanol for five minutes before subsequent sonication with 30% acetonitrile, 0.1% TFA solution for a further five minutes. Targets were then washed briefly with HPLC grade methanol before drying by nitrogen gas.

Sample preparation for MALDI-TOF MS analysis. Cell pellets were processed in one of three ways:

(a) Direct analysis where cell pellets were washed twice with PBS and centrifuged at 300 xg, 4 °C for 10 minutes. Cell pellets were then resuspended in 0.1% TFA before subsequent spotting.

(b) Cell pellets were snap frozen on dry ice and stored at -80°C until required. Cell pellets were then thawed and centrifuged at 300 xg, 4 °C for 10 minutes before being resuspended in a choice of solvent: hexane, dichloromethane, acetone, methanol, acetonitrile, phosphate buffered saline (PBS) or water pH 7. Cell suspensions were then centrifuged at 300 xg, 4°C for 10 minutes before being resuspended in 0.1% TFA.

(c) Cell pellets were resuspended in a choice of solvent (hexane, dichloromethane, acetone, methanol, acetonitrile, phosphate buffered saline or water) before centrifugation at 300 xg, 4°C for 10 minutes. Cell pellets were then resuspended in 0.1% TFA and snap frozen on dry ice and stored at -80°C until required.

Matrix preparation and spotting. Sinapinic Acid (SA), α-cyano-4-hydroxycinnamic acid (CHCA) and dihydroxybenzoic acid (DHB) were used as matrices for all MALDI-TOF cellular analysis. All matrix solutions were prepared in 50% ACN, 0.1% TFA at varying concentrations and ratios of matrix solute: 2.5, 10, 20 mg/mL or saturated. For manual deposition cell suspensions were mixed at a 1:1 ratio with matrix solution and 1 µL spotted onto a ground steel MALDI target before ambient drying.

Automated target spotting was performed using a Mosquito liquid handling robot (TTP Labtech) by first aliquoting 200 nL of matrix solution onto an AnchorChip MALDI target and after drying 200 nL of cell suspension deposited on top. Finally, 200

nL of matrix was further deposited onto dried spots to create a "sandwich" spot and the target allowed to ambient dry before analysis.

MALDI-TOF MS analysis. A RapifleX PharmaPulse MALDI TOF/TOF mass spectrometer (Bruker Daltonics) equipped with a Smartbeam 3D laser was used in positive ion mode with Compass 2.0 control for all data acquisition. Samples were acquired in automatic mode (AutoXecute; Bruker Daltonics), totaling 10,000 shots at a 10-kHz frequency per spot with a random walk (complete sample) on spot laser ablation pattern and M5 Smart beam Parameter at a 45-µm × 45-µm scan range. Ionization was achieved using a variable laser power between 50-85% (laser attenuator offset 14%, range 30%) with a detector gain of ×6.8 in the 2000 to 20,000 *m/z* mass range with a mass suppression up to 1600 *m/z*. Samples were analyzed in a linear geometry with optimized voltages for ion sources (ion source 1, 20 kV, PIE 1.3 kV), lens (8.6 kV), and a pulsed ion extraction of 180 ns. A novel 10-bit digitizer was used at a sampling rate of 1.25 GS/s. Raw data were processed first by a TopHat baseline subtraction followed by smoothing with a SavitzkyGolay algorithm. MALDI TOF data processed by the FlexAnalysis 4.0 software where a peak picking threshold of 3 S/N was set before being exported as a .csv file using FlexAnalysis Batch Process (Compass 2.0) and further processed in Microsoft Excel and/or Perseus.[39] Spectra based PCA plots were generated using ClinPro Tools (Bruker Daltonics). Data was then formatted using both GraphPad Prism 7.0 and Adobe Illustrator.

Perseus analysis of mESCs. Raw data were first separated into their corresponding biological and technical replicates with reported relative intensity (Supp. Table 1). A complete matrix was imported into Perseus (v.1.6.0.7) and data was filtered so that only features that were identified in 10 spectra in total were selected. This filtered mass list was then used to generate PCA plots using Perseus. Z-score averaging was performed on the filtered data set and included unique peaks identified to each of the two conditions. Hierarchical clustering was performed with Euclidian distancing and 20 and 10 number of clusters for row and column trees respectively.

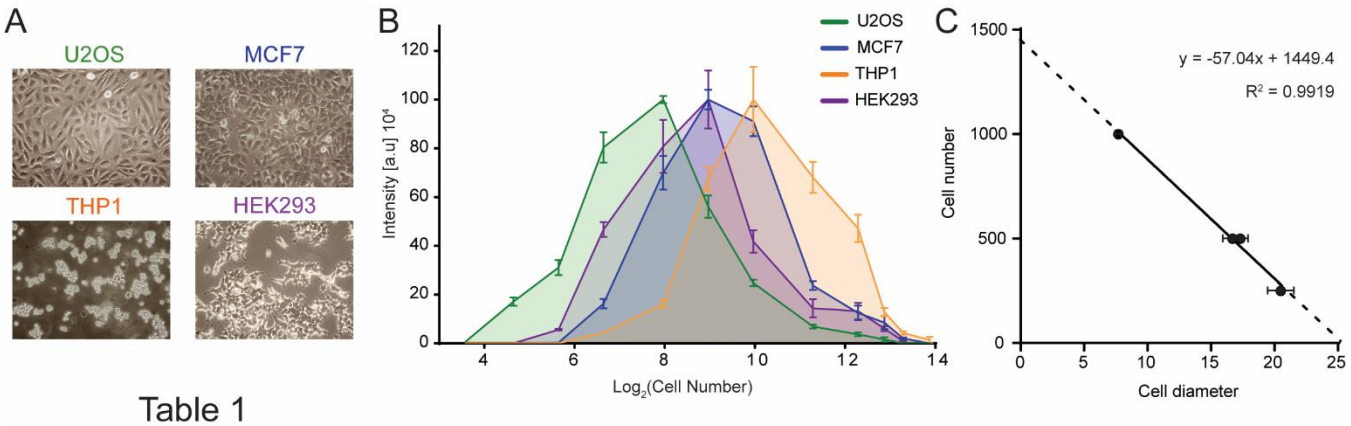

Table 1

Cell line	**U2OS**	**MCF7**	**THP1**	**HEK293**
Cell diameter (µm)	21.6 ± 1.4	18.1 ± 0.75	8.0 ± 0.25	16.9 ± 0.63
Optimal cell number	250	500	1000	500

Figure 1: Optimizing cell numbers for whole cell MALDI-TOF MS. (A) Light microscopy images of four human cell lines U2OS, MCF7, THP1 and HEK293. (B) 2D plot of normalized mass spectrum intensity at different cell numbers on target for each of the four cell lines. Plots have maxima indicating optimal cell numbers. (C) Plotting optimal cell numbers derived from (B) against their respective measured cell diameter shows a high correlation. Plots in (B) derived from 6 technical replicates. Error bars represent standard deviation. Table 2 measured diameter of each cell line with standard deviation as well as optimal cell number on spot derived from the titration.

Results and Discussion

Optimizing the workflow for mammalian cell MALDI-TOF MS. In order to optimize the sample preparation for whole cell MALDI-TOF MS, we focused initially on four different human cell lines (U2OS, MCF7, THP1 and HEK293) (Figure 1A). Cells were washed once with PBS to remove the culture medium, as high levels of fetal bovine serum (FBS) and salts from the culture medium affect MALDI-TOF MS ionization. To determine optimal cell concentration, we spotted 25 to 20,000 cells on target. Surprisingly, there was a narrow window where good spectra could be acquired, with large numbers of cells on-spot proving to be detrimental to ionization. We believe that this is due to increasing amounts of salts and unfavorable biomolecules on-spot with increasing numbers of cells. Further to this, we observed that the best spectral intensity varied for each cell line (Figure 1B) and hypothesized that the number of ionizable biomolecules from cells was dependent on the cell size. Therefore, we measured the diameters of all four cells lines in solution (Table 1) and plotted these values against the optimal cell number derived from the titration to identify an optimal cells number on-target for MALDI-TOF MS analysis (Figure 1C). This generated a linear relationship with a very good correlation of $R^2 = 0.99$ indicating that to obtain optimal and reproducible

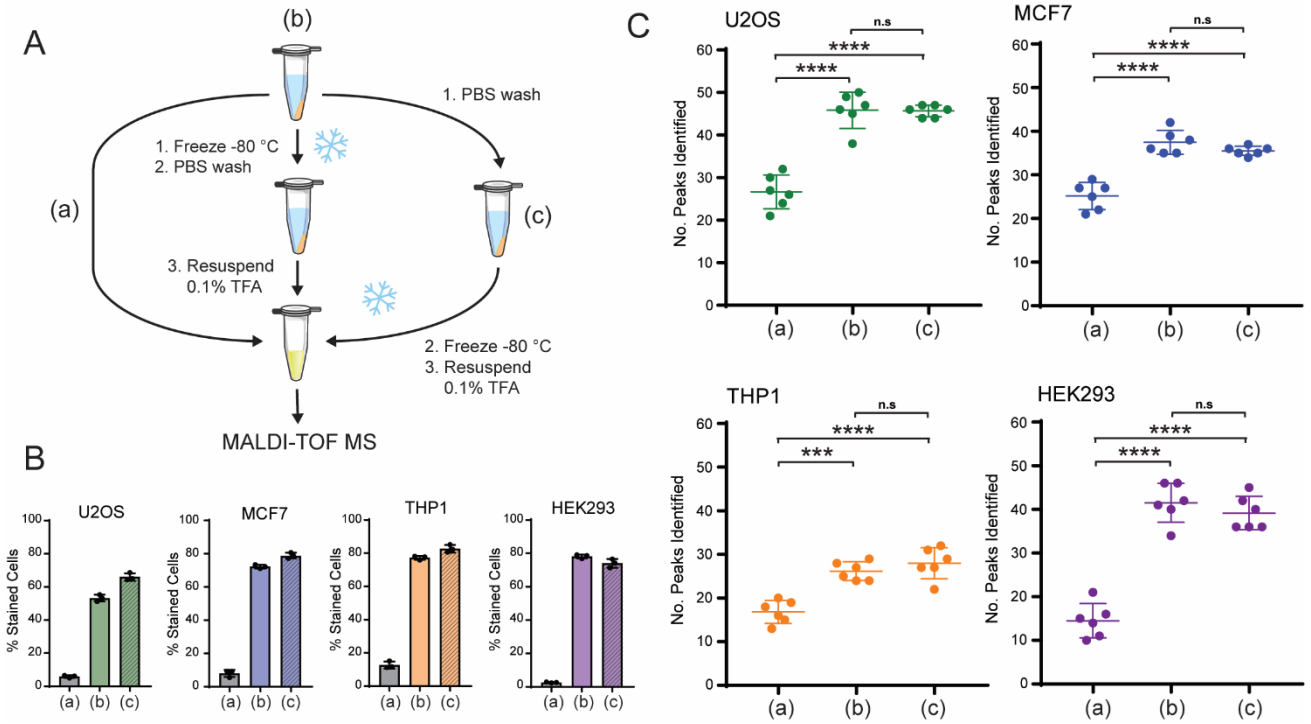

Figure 2. Freeze/thawing enhances number of peaks identified from whole cells. (A) Schematic showing workflow. (B) Trypan blue staining of the four cell lines shows that the freeze/thaw cycle significantly increases percentage of trypan blue positive cells and therefore cell membrane permeability. (C) Number of peaks identified across six technical replicates for each of the experimental workflows shown in (A). Data show that the number of features identified are significantly increased upon inclusion of a freeze/thaw cycle. Error bars represent standard deviation of six replicates. *** and **** represent $p<0.001$ and $p<0.0001$, respectively, student's t-test.

spectra from mammalian cells by MALDI-TOF MS, cell numbers need to be optimized and this number is dependent on cell size.

We tested next, if the biomolecules detected from mammalian cells derive from intact cells or if mild breakage of cells enhanced the occurrence of unique mass features. In our experience, harsh lysing conditions resulted in spectra that were less distinguishable (data not shown), which has also been observed by lysing with increasing acidity.34 It was indicated before that freeze-thawing of cell pellets prior to MALDI-TOF MS analysis has beneficial effects with respect to number of features identified and overall spectral intensity.31,40 This is likely due to the freeze/thaw cycle permeating the cell membrane, thus allowing the cytoplasmic contents of the cells to become exposed and more easily ionized. We therefore decided to test whether a freeze/thaw cycle improved MALDI-TOF MS analysis of mammalian cell lines and whether freezing before or after a wash with PBS affected sensitivity and spectral quality compared with direct analysis (Figure 2A). We first validated that both methods of freezing permeated the cell membrane by measuring the percentage of stained cells when treated with trypan blue (Figure 2B). Freeze-thawing led to permeabilization of about 50-80% of the cells with both strategies (Figure 2B) and we observed a significant increase in the number of peaks identified compared to "intact" cell samples (Figure 2C). As well as this, software analysis did not result in a significant difference between cells frozen before or after further treatment and manual inspection of spectra resulted in the same conclusion (Figure S-1). We conclude that a freeze/thaw cycle is critical to improve MALDI-TOF MS quality of mammalian cells as it increases the number of features identified. However, the order in which this step is performed, does not affect the final readout.

Solvent wash vs direct analysis of mammalian cells. Next, we examined how different solvent-extraction techniques influence the preparation of mammalian cells for MALDI-TOF MS analysis. Covering a large polar range, we chose to test seven different solvent washes (Figure 3A). Some of these conditions have already been described in the literature for bacterial biotyping or are routinely used in cell preparations for other analyses such as methanol fixing for microscopy studies.[41] We systematically evaluated how well each solvent extraction method performed with respect to the number of identified peaks, quality of the acquired spectra, as well as technical reproducibility when analyzed by MALDI-TOF MS.

Each extraction method distinguished each of the four cell lines by both manual spectra interrogation and principle component analysis (PCA) (Figure 3D & E, S-2). It is interesting to note that the apolar solvents appeared to group closer together and were therefore more similar (Figure S-3). However, each extraction method was able to generate a unique set of peaks for each of the four cell lines, thus allowing classification of the different populations (Figure 3B & C, S-2). The three most apolar solvents identified the lowest number of features for each of the four cell lines (Figure 3F & G, S-2) so we focused on the four remaining methods: methanol, acetonitrile, PBS and water. We observed that for acetonitrile, one peak at 4950 *m/z* dominated in intensity across the acquired spectra. We therefore looked at how the relative intensity of peaks was distributed for the top 10 most intense peaks for each cell line and each extraction method (Figure 3H & I, S-2). This is important for high-throughput analysis, as peaks identified with a lower S/N and intensity are less likely to be quantified accurately. The peak at 4950 *m/z* in the acetonitrile treated THP1 and U2OS samples contributed to almost 50% of the intensity of the spectra,

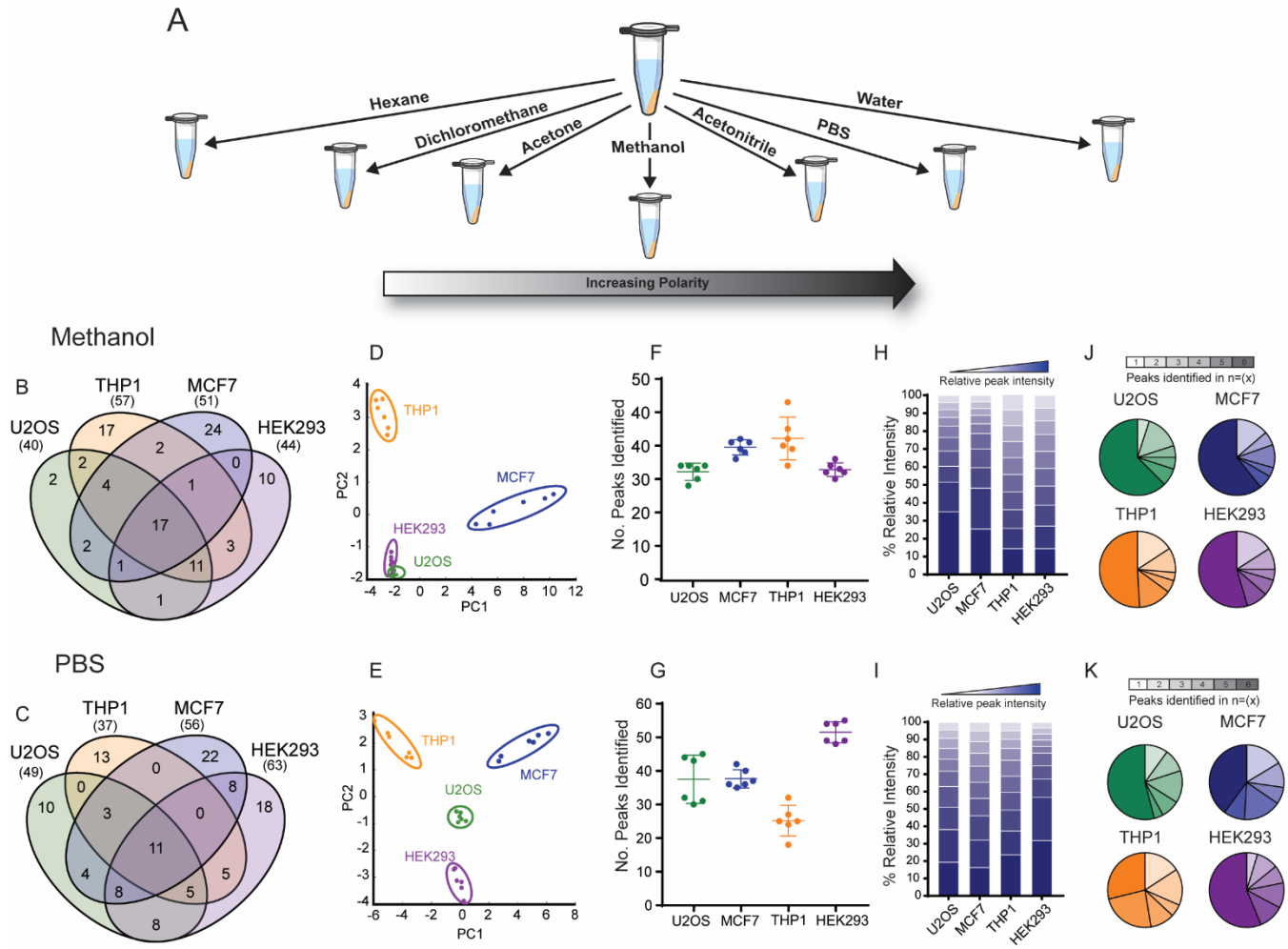

Figure 3: Methanol and PBS washes are best to identify reproducible features in whole cell MALDI-TOF MS. (A) Schematic of the different solvent washes performed with respect to their increasing polarity. (B & C) Number of identified unique features for any of the four cells after methanol (B) and PBS (C) washes. (D & E) PCA plots showing how multivariate analysis can distinguish each of the four cell lines after methanol (D) and PBS (E) washes. (F & G) Number of peaks identified for each cell line over six technical replicates. (H & I) Relative intensity distribution of the top 10 peaks identified over six technical replicates for each cell line. (J & K) Pie charts displaying the % of peaks identified within each of the six replicates per cell line.

whereas the other three solvents showed a more even intensity distribution. Finally, and arguably most importantly, we looked at how reproducible peaks were identified over six technical replicates (Figure 3J & K, S-2). Methanol was the most consistent, with the majority of all peaks being identified in all six spectra, whereas PBS and water (pH 7) were slightly more variable. Taken together, our data suggests that washing cells with either methanol or PBS generated the best and least variable spectra in mammalian cell MALDI-TOF MS.

Choosing a suitable matrix for mammalian cell MALDI-TOF MS. Following the optimization of the washing method, we tested which type of matrix allows for the best MALDI-TOF MS analysis of mammalian cells. The three matrices mostly used in MALDI-TOF MS are sinapinic acid (SA), α-cyano-4-hydroxycinnamic acid (CHCA) and dihydroxybenzoic acid (DHB), which are often categorized for the analysis of proteins, peptides, and glycans, lipids and peptides, respectively. However, when analyzing whole mammalian cells by MALDI-TOF MS the origin of the biomolecules being ionized is often unknown, and we therefore hypothesized that the choice of matrix will have a significant influence on the resulting mass spectrum.

As expected, when each cell line sample was prepared with either saturated SA, CHCA and DHB, dramatically different mass profiles of the same cell line were observed (Figure S-6), which could be distinguished by PCA (Figure 4A). Using DHB matrix resulted in more variable spectra over technical replicates, with the PCA analysis using ClinPro Tools software showing wider distances and grouping only three of the six technical replicate spectra for MCF7 cells. Moreover, we could classify unique peaks to each of the matrices (Figure S-7), which indicates that different biomolecules are being ionized and mammalian cell profiles are matrix-dependent. As it is paramount for successful phenotypic or compound library screening that unique features must be routinely and robustly detected, we firstly assessed the reproducibility of identified features over six technical replicates for each matrix (Figure S-7). Both CHCA and SA were the most consistent with respect to peak reproducibility, whereas DHB performed poorly in comparison, with only a maximum of 40% of peaks being reproducible in half the technical replicates, and less than 10% when analyzing HEK293. This was somewhat expected as DHB is known to produce large, needle-like crystals and combined with highly complex samples, such as mammalian cells, this resulted in an irreproducible spotting method.

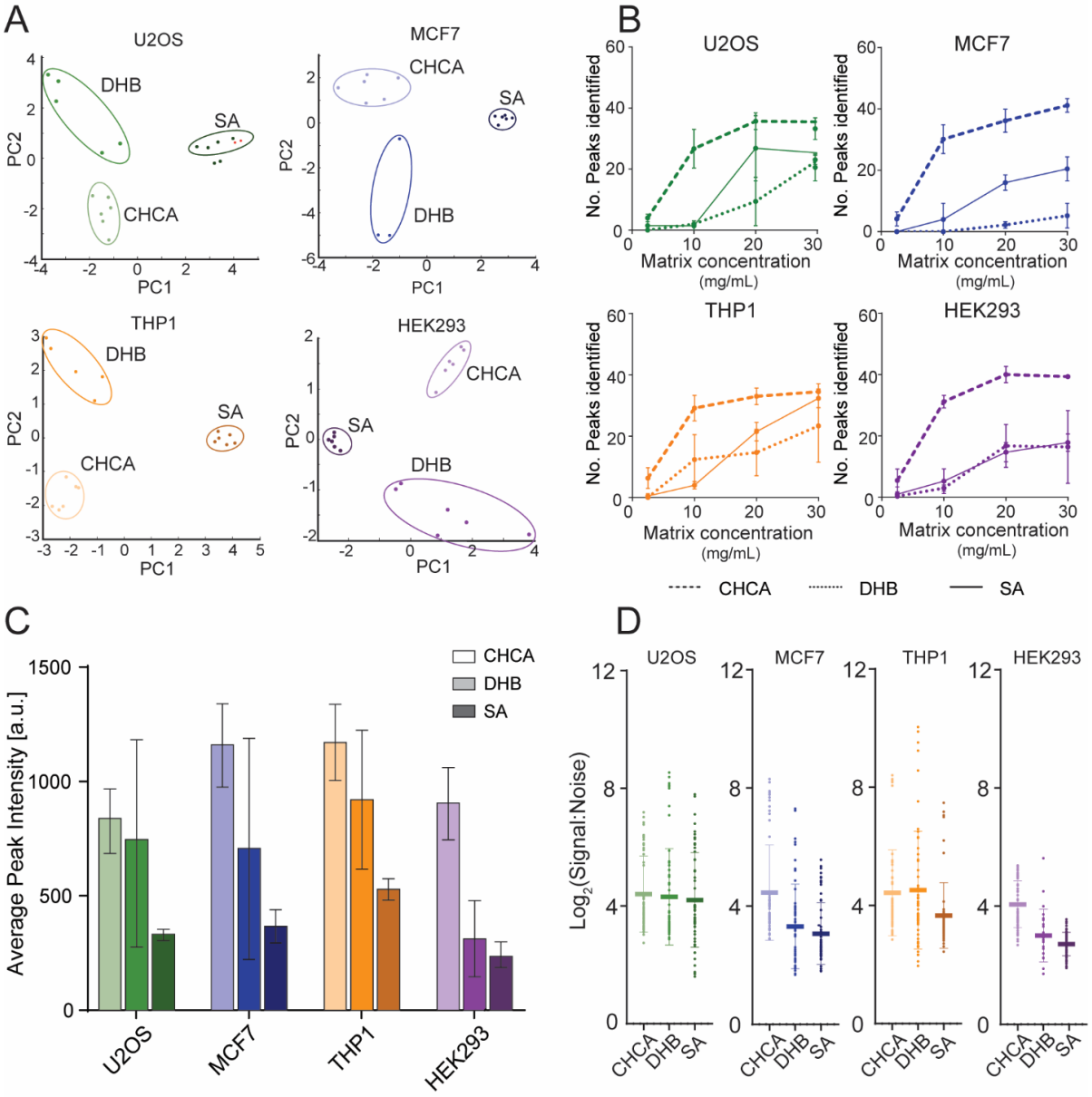

Figure 4: CHCA performs best for whole cell MALDI-TOF MS. (A) Dependence of matrix concentration on number of peaks identified for each of the four human cell lines and three matrices. (B) Average peak intensity is dependent on matrix choice (CHCA> DHB> SA) for each of the four cell lines. (C) Log_2 signal to noise (S/N) of the top 10 peaks identified in each of the six replicates for the four cell lines shows that peak S/N is lower in SA compared to CHCA and DHB. Error bars represent standard deviation of six replicates.

We also chose to look at other important parameters for peak identification, such as matrix concentration, peak intensity and signal to noise (S:N), to assess suitability of matrices for mammalian cell analysis. CHCA and SA outperformed DHB with respect to the number of features identified for each cell line. Although all matrices performed best when saturated, a lower concentrated solution of CHCA still produced dramatically better results compared to SA and DHB (Figure 4B). This was surprising as most publications in mammalian cell MALDI-TOF MS analysis used SA in the past.[34,40,42] Yet, despite having the tightest PCA grouping (Figure 4A), this matrix performed poorly in other areas. Spectra acquired using SA had very low intensity compared to CHCA and DHB (Figure 4C), and this trend was similarly observed for top-10 peak signal to noise, where significantly more peaks were identified with a lower S:N value (Figure 4D). Taken together, our results show that CHCA is the most suitable matrix not only for generating MALDI-TOF MS fingerprints of mammalian cells, but also for analyses requiring more throughput, as it outperforms DHB and SA for technical reproducibility and spectral quality and can be used at lower concentrations.

MALDI-TOF MS profiling of pharmacologically controlled stem cell differentiation. Finally, we wanted to apply our optimized parameters to phenotypically profile cells in an physiologically relevant system that is employed in drug screening and toxicity testing and that has been used as a drug discovery model.[43] We used mouse embryonic stem cells (mESC) maintained in a naïve ground state pluripotency using the 2i kinase inhibitor system (PD0325901 and CHIR99021), which inhibit the kinases ERK1/2 and GSK3, respectively (Figure 5A & C).[37,44]

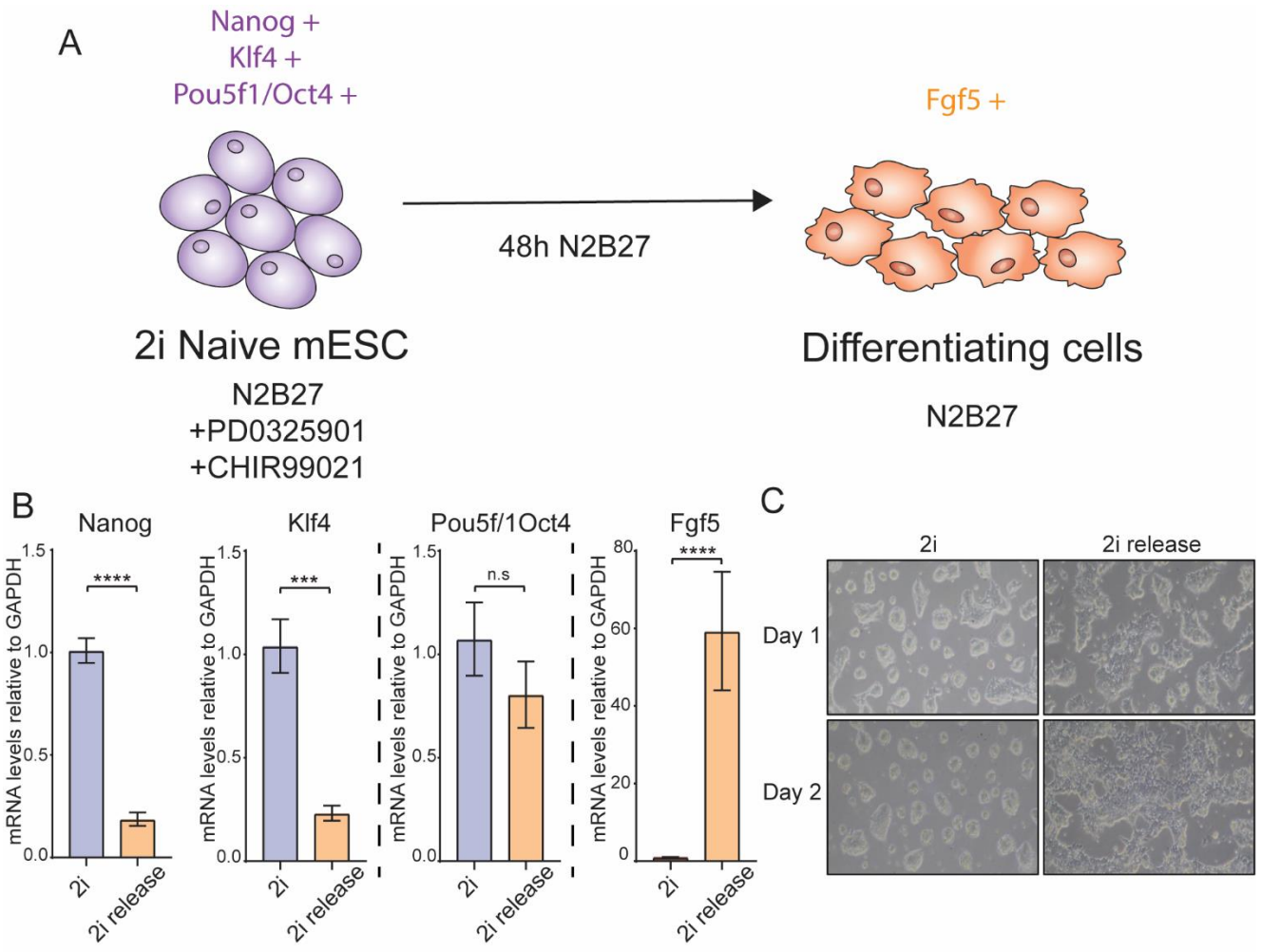

Figure 5: Differentiation of naïve ground state mESCs. (A) Schematic showing the differentiation of naïve mESCs upon removal of the two kinase inhibitors (2i). (B) qPCR data showing changes in key mESC pluripotency and differentiation genes. (C) Light microscopy image showing the morphological change in naïve mESCs upon 2i release after 1 and 2 days. Error bars represent standard deviation of 2 technical replicates from 3 biological replicates X replicates. *** and **** represent $p<0.001$ and $p<0.0001$, respectively, student's t-test.

We tested whether we could distinguish cellular phenotypic changes upon release from 2i into N2B27 media alone, which drives efficient multi-lineage differentiation.[38] We processed three biological and five technical replicates of 2i and 2i release conditions using the optimized parameters above.

Table 2. Relative intensity fold change of selected peaks

m/z	Relative fold increase	
	2i	2i release
2437.4	x	2.03
5438.3	x	2.70
7148.8	x	2.08
7412.4	x	8.82
3097.2	4.57	x
4628.1	2.34	x
6197.1	3.18	x
11174.5	2.86	x

Efficient exit from naïve ground state pluripotency towards differentiation upon 2i release was confirmed by suppressed mRNA expression of the naïve pluripotency factors *Nanog* and *Klf4*, and induction of the lineage priming/differentiation marker *Fgf5* (Figure 5B). As expected, the pluripotency factor Pou5f1/Oct4, which is expressed in both naïve and lineage primed mESC states, is not significantly altered upon acute 2i release (Figure 5B).We could robustly identify unique features to each population, as well as quantify changes in common peaks. For all spectra, the base peak was identified at *m/z* 4875.20, which made subsequent analysis simpler, as the raw spectral intensity can vary significantly from spot-to-spot. Utilizing *m/z* 4875.20, as a normalizing control, we identified common features reported in Table 3 that exhibited a fold increase greater than two in peak area in both 2i and 2i release conditions (Figure. 6A. T-3). We identified a number of peaks that were unique to 2i and 2i release, such as *m/z* 5566.78 and *m/z* 3282.06, respectively (Figure 6A).

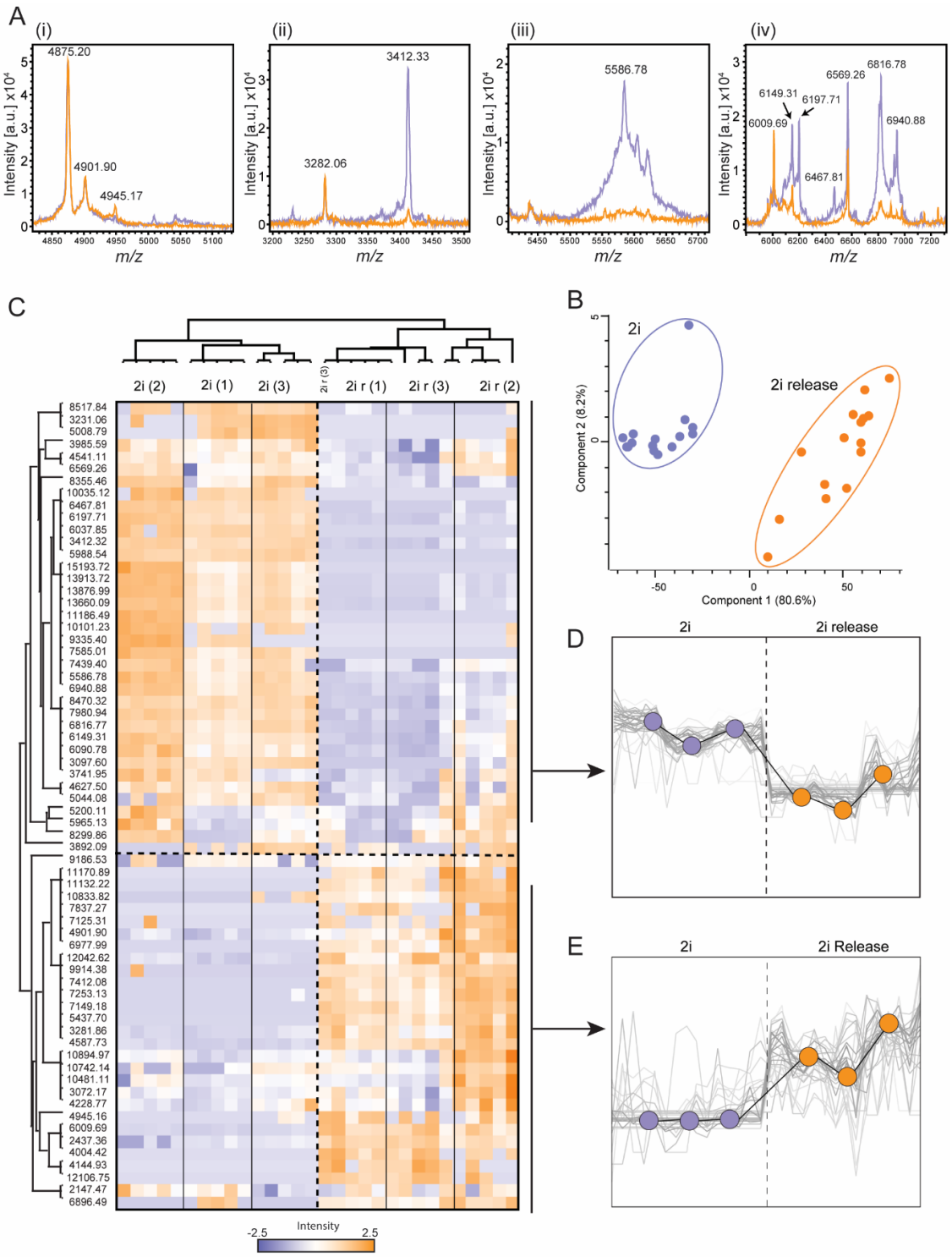

Figure 6: Whole cell MALDI-TOF MS distinguishes between naïve and differentiating mESCs. (A) Selected examples of mass spectral regions that showed changes between mESCs cultured in 2i and 2i release conditions where the base peak (4950 *m/z*) is of identical intensity, thus allowing intensity comparison. (B) PCA plot showing how the two cell populations can be distinguished by multivariate analysis over three biological and five technical replicates. (C) Z'-score heat map showing how each normalized peak intensity changes with respect to 2i and 2i release condition over three biological and five technical replicates. (D) Cluster profiles of the two cell populations and how their normalized intensity trends can be distinguished.

2i and 2i release conditions could be well differentiated as two populations by PCA (Figure 6B) and we observed good grouping of biological replicates. To further understand how relative intensity of specific peaks changed across the three biological and five technical replicates, we generated a Z-score heatmap of detected mass features (Figure 6C). This hierarchical clustering approach allowed us to look at the unique and common features combined across all independent biological and technical replicates. The three biological replicates clustered well together and 2i and 2i release conditions were separated efficiently. From the heatmap, we were able to generate two discrete row clusters – peaks that were up-regulated and those that were down-regulated upon release from PD0325901 and CHIR99021 inhibitors (Figure

6E & F). Through this, we identified several peaks that reproducibly changed significantly between the conditions and these can now be used as markers of phenotypic screening of mESC differentiation (Table 3).

Conclusion

Due to its speed and its relative simplicity, MALDI-TOF MS has become increasingly popular for the application of bacterial biotyping. However, a complimentary methodical approach to phenotypic screening of mammalian cells has not been well characterized. Here we presented a systematic study that addresses three of the key steps in sample preparation of mammalian cells for MALDI-TOF-MS analysis: cell culture and harvesting, the use of an extraction technique and matrix choice. We found that at all three steps had a profound impact on the resulting mass spectra and subsequent data analysis. We also applied a unique way of analyzing the efficacy of each method by looking at not only spectral quality and observable changes but evaluating performance over technical replicate spots. This enabled us to gain a deeper understanding of how each step of the sample preparation impacts subsequent analysis and consequently an insight as to how each method would perform with higher throughput analyses. Our optimized method was validated by our observation of distinct MALDI-TOF MS profiles for naïve ground state mESCs compared to differentiating mESCs in a pharmacologically controlled system. Using hierarchical clustering, we could visualize and identify a subset of peaks that are unique to each condition. We therefore present here a novel sample preparation method that enables robust, reproducible and rapid profiling of mammalian cells and is suitable for expansion to high-throughput platform.

ASSOCIATED CONTENT

Supporting Information

Supplementary figures, tables and texts (PDF)
Complete Table of 2i and 2i release relative intensities (.xlsx)

AUTHOR INFORMATION

Corresponding Author

*Email: Matthias.trost@newcastle.ac.uk; phone: +44 191 2087009

Author Contributions

The manuscript was written through contributions of all authors. / All authors have given approval to the final version of the manuscript.

Notes

The authors declared no potential conflicts of interest with respect to the research, authorship, and/or publication of this article.

ACKNOWLEDGMENT

We thank the Bruker Daltonics, particularly Meike Hamester, Anja Resemannd and Astrid Erdmann, for their support. We thank Anetta Härtlova, Adam Moore, Shin Lim and Julien Peltier for help. The authors disclosed receipt of the following financial support for the research, authorship, and/or publication of this article: This work was funded by generous start-up funds from Newcastle University to MT, an iCASE studentship to REH by the BBSRC and Bruker Daltonics. GMF is funded by a Wellcome Trust/Royal Society Sir Henry Dale Fellowship, ASF is supported by a studentship from the MRC.

REFERENCES

(1) Pappin, D. J.; Hojrup, P.; Bleasby, A. *Curr. Biol.* **1993**, *3*, 327–332.
(2) Cohen, L. H.; Gusev, A. I. *Anal Bioanal Chem* **2002**, *373*, 571–586.
(3) Aichler, M.; Walch, A. *Laboratory Investigation* **2015**, *95*, 422–431.
(4) Haslam, C.; Hellicar, J.; Dunn, A.; Fuetterer, A.; Hardy, N.; Marshall, P.; Paape, R.; Pemberton, M.; Resemannand, A.; Leveridge, M. *J Biomol Screen* **2016**, *21*
(5) Chandler, J.; Haslam, C.; Hardy, N.; Leveridge, M.; Marshall, P. *SLAS Discov* **2017**, *22* (10), 1262–1269.
(6) Winter, M.; Ries, R.; Kleiner, C.; Bischoff, D.; Luippold, A. H.; Bretschneider, T.; Büttner, F. H. *SLAS TECHNOLOGY: Translating Life Sciences Innovation* **2018**
(7) Ritorto, M. S.; Ewan, R.; Perez-Oliva, A. B.; Knebel, A.; Buhrlage, S. J.; Wightman, M.; Kelly, S. M.; Wood, N. T.; Virdee, S.; Gray, N. S.; et al. *Nature Communications* **2014**, *5*, 4763.
(8) Cesare, V. D.; Johnson, C.; Barlow, V.; Hastie, J.; Knebel, A.; Trost, M. *Cell Chemical Biology* **2018**, *0*
(9) Heap, R. E.; Hope, A. G.; Pearson, L.-A.; Reyskens, K. M. S. E.; McElroy, S. P.; Hastie, C. J.; Porter, D. W.; Arthur, J. S. C.; Gray, D. W.; Trost, M. *SLAS Discov* **2017**, *22*, 1193–1202.
(10) Winter, M.; Bretschneider, T.; Kleiner, C.; Ries, R.; Hehn, J. P.; Redemann, N.; Luippold, A. H.; Bischoff, D.; Büttner, F. H. *SLAS Discov* **2018**, *23*, 561–573.
(11) Guitot, K.; Drujon, T.; Burlina, F.; Sagan, S.; Beaupierre, S.; Pamlard, O.; Dodd, R. H.; Guillou, C.; Bolbach, G.; Sachon, E.; et al. *Analytical and Bioanalytical Chemistry* **2017**, *409*, 3767–3777.
(12) Guitot, K.; Scarabelli, S.; Drujon, T.; Bolbach, G.; Amoura, M.; Burlina, F.; Jeltsch, A.; Sagan, S.; Guianvarc'h, D. *Analytical Biochemistry* **2014**, *456*, 25–31.
(13) Gurard-Levin, Z. A.; Scholle, M. D.; Eisenberg, A. H.; Mrksich, M. *ACS Comb Sci* **2011**, *13* (4), 347–350.
(14) Patel, K.; Sherrill, J.; Mrksich, M.; Scholle, M. D. *J Biomol Screen* **2015**, *20* (7), 842–848.
(15) O'Kane, P. T.; Mrksich, M. *J. Am. Chem. Soc.* **2017**, *139* (30), 10320–10327.
(16) Wood, S. E.; Sinsinbar, G.; Gudlur, S.; Nallani, M.; Huang, C.-F.; Liedberg, B.; Mrksich, M. *Angew. Chem. Int. Ed. Engl.* **2017**, *56* (52), 16531–16535
(17) Ban, L.; Pettit, N.; Li, L.; Stuparu, A. D.; Cai, L.; Chen, W.; Guan, W.; Han, W.; Wang, P. G.; Mrksich, M. *Nat. Chem. Biol.* **2012**, *8* (9), 769–773.
(18) Fenselau, C.; Demirev, P. A. *Mass Spectrom Rev* **2001**, *20* (4), 157–171.
(19) Croxatto, A.; Prod'hom, G.; Greub, G. *FEMS Microbiol Rev* **2012**, *36* (2), 380–407.
(20) Claydon, M. A.; Davey, S. N.; Edwards-Jones, V.; Gordon, D. B. *Nat. Biotechnol.* **1996**, *14* (11), 1584–1586.
(21) Holland, R. D.; Wilkes, J. G.; Rafii, F.; Sutherland, J. B.; Persons, C. C.; Voorhees, K. J.; Lay, J. O. *Rapid Commun. Mass Spectrom.* **1996**, *10* (10), 1227–1232.
(22) Wang, Z.; Dunlop, K.; Long, S. R.; Li, L. *Anal. Chem.* **2002**, *74* (13), 3174–3182.
(23) Rahi, P.; Prakash, O.; Shouche, Y. S. *Front Microbiol* **2016**, *7*.
(24) Jarman, K. H.; Cebula, S. T.; Saenz, A. J.; Petersen, C. E.; Valentine, N. B.; Kingsley, M. T.; Wahl, K. L. *Anal. Chem.* **2000**, *72* (6), 1217–1223.
(25) Williams, T. L.; Andrzejewski, D.; Lay, J. O.; Musser, S. M.. *Journal of the American Society for Mass Spectrometry* **2003**, *14* (4), 342–351.
(26) Wunschel, S. C.; Jarman, K. H.; Petersen, C. E.; Valentine, N. B.; Wahl, K. L.; Schauki, D.; Jackman, J.; Nelson, C. P.; White, E. *Journal of the American Society for Mass Spectrometry* **2005**, *16* (4), 456–462.
(27) Alatoom, A. A.; Cunningham, S. A.; Ihde, S. M.; Mandrekar, J.; Patel, R. *J. Clin. Microbiol.* **2011**, *49* (8), 2868–2873.
(28) Toh-Boyo, G. M.; Wulff, S. S.; Basile, F. *Anal. Chem.* **2012**, *84* (22), 9971–9980.
(29) Bizzini, A.; Durussel, C.; Bille, J.; Greub, G.; Prod'hom, G. *J Clin Microbiol* **2010**, *48* (5), 1549–1554.

(30) Serafim, V.; Shah, A.; Puiu, M.; Andreescu, N.; Coricovac, D.; Nosyrev, A.; Spandidos, D. A.; Tsatsakis, A. M.; Dehelean, C.; Pinzaru, I. *Int. J. Mol. Med.* **2017**, *40* (4), 1096–1104.

(31) Chen, X.; Wo, F.; Chen, J.; Tan, J.; Wang, T.; Liang, X.; Wu, J. *Scientific Reports* **2017**, *7* (1).

(32) Holzlechner, M.; Strasser, K.; Zareva, E.; Steinhäuser, L.; Birnleitner, H.; Beer, A.; Bergmann, M.; Oehler, R.; Marchetti-Deschmann, M. *Journal of Proteome Research* **2017**, *16* (1), 65–76.

(33) Ouedraogo, R.; Flaudrops, C.; Ben Amara, A.; Capo, C.; Raoult, D.; Mege, J.-L. *PLoS ONE* **2010**, *5* (10),

(34) Munteanu, B.; von Reitzenstein, C.; Hänsch, G. M.; Meyer, B.; Hopf, C. *Anal Bioanal Chem* **2012**, *404* (8), 2277–2286.

(35) Portevin, D.; Pflüger, V.; Otieno, P.; Brunisholz, R.; Vogel, G.; Daubenberger, C. *BMC Biotechnol* **2015**, *15*.

(36) Ouedraogo, R.; Daumas, A.; Ghigo, E.; Capo, C.; Mege, J.-L.; Textoris, J. *Journal of Proteomics* **2012**, *75* (18), 5523–5532.

(37) Ying, Q.-L.; Wray, J.; Nichols, J.; Batlle-Morera, L.; Doble, B.; Woodgett, J.; Cohen, P.; Smith, A. *Nature* **2008**, *453* (7194), 519–523.

(38) Kalkan, T.; Olova, N.; Roode, M.; Mulas, C.; Lee, H. J.; Nett, I.; Marks, H.; Walker, R.; Stunnenberg, H. G.; Lilley, K. S.; et al. *Development* **2017**, *144* (7), 1221–1234.

(39) Tyanova, S.; Temu, T.; Cox, J. *Nature Protocols*. **2016**, 11, 2301-2319

(40) Schwamb, S.; Munteanu, B.; Meyer, B.; Hopf, C.; Hafner, M.; Wiedemann, P. *J. Biotechnol.* **2013**, *168* (4), 452–461.

(41) Suthipintawong, C.; Leong, A. S.; Vinyuvat, S. *Diagn. Cytopathol.* **1996**, *15* (2), 167–174.

(42) Kober, S. L.; Meyer-Alert, H.; Grienitz, D.; Hollert, H.; Frohme, M. *Analytical and Bioanalytical Chemistry* **2015**, *407* (25), 7721–7731.

(43) Pouton, C. W.; Haynes, J. M. *Nature Reviews Drug Discovery* **2007**, *6* (8), 605–616.

(44) Silva, J.; Barrandon, O.; Nichols, J.; Kawaguchi, J.; Theunissen, T. W.; Smith, A. *PLOS Biology* **2008**, *6* (10)

Insert Table of Contents artwork here